Geophysical Research Letters

RESEARCH LETTER
10.1029/2022GL098806

Deciphering the Migration of the Intertropical Convergence Zone During the Last Deglaciation

Shouwei Li[1] **and Wei Liu**[1]

[1]Department of Earth and Planetary Sciences, University of California Riverside, Riverside, CA, USA

Key Points:

- The intertropical convergence zone (ITCZ) abruptly shifts southward during Heinrich Stadial 1 (HS1) and Younger Dryas against a long-term trend of northward migration during the last deglaciation
- Driven by meltwater, changes in top-of-atmosphere (TOA) radiation and global oceanic heat transport have nearly equivalent impacts on ITCZ shift during HS1
- Ice sheet extent changes cause a large interhemispheric TOA radiation asymmetry during HS1 but not via the surface albedo feedback

Supporting Information:

Supporting Information may be found in the online version of this article.

Correspondence to:

S. Li,
sli227@ucr.edu

Citation:

Li, S., & Liu, W. (2022). Deciphering the migration of the intertropical convergence zone during the last deglaciation. *Geophysical Research Letters*, *49*, e2022GL098806. https://doi.org/10.1029/2022GL098806

Received 12 JAN 2022
Accepted 28 APR 2022

Author Contributions:

Conceptualization: Shouwei Li, Wei Liu
Formal analysis: Shouwei Li
Methodology: Shouwei Li
Validation: Wei Liu
Visualization: Shouwei Li
Writing – original draft: Shouwei Li
Writing – review & editing: Wei Liu

Abstract Proxy evidences suggest abrupt southward displacements of the intertropical convergence zone (ITCZ) during Heinrich Stadial 1 (HS1) and Younger Dryas (YD) against a long-term trend of northward ITCZ migration from Last Glacial Maximum to modern climate. Climate model simulations reveal that the abrupt ITCZ changes in HS1 and YD are mainly driven by ice-sheet-induced meltwater while the long-term ITCZ trend primarily results from orbital variations, rising atmospheric greenhouse gases and ice-sheet retreats during the last deglaciation. Atmospheric energetics analysis elucidates two important processes driven by meltwater—less net radiation entering the top-of-atmosphere (TOA) in the Northern Hemisphere than the Southern Hemisphere and a reduced global cross-equatorial oceanic heat transport from the compensation between Atlantic and Indo-Pacific heat transports—induce the southward ITCZ shift during HS1. Ice sheet extent changes also create a large interhemispheric TOA radiation asymmetry during HS1, which, however, is not via the surface albedo feedback.

Plain Language Summary We explore the change in tropical rainbelt during the last deglaciation based on proxy data and climate model simulations. We find two types of changes, the abrupt southward shifts of tropical rainbelt during two periods of the so-called Heinrich Stadial 1 (HS1) and Younger Dryas and a long-term shift trend of tropical rainbelt from Last Glacial Maximum to modern climate. The former change can be mainly attributed to ice-sheet-induced meltwater while the latter change can be mainly attributed to orbital variations, increasing atmospheric greenhouse gases and ice-sheet retreats. Our further analysis shows that, driven by meltwater, changes in both top-of-atmosphere (TOA) radiation and global oceanic heat transport have almost equivalent impacts on the southward shift of tropical rainbelt during HS1. Besides, ice sheet extent changes can generate a large interhemispheric TOA radiation asymmetry during HS1 but not via the surface albedo feedback.

1. Introduction

Paleo-evidences suggest pronounced changes in global hydroclimate and global monsoon system during the last deglaciation (Clark et al., 2012; Geen et al., 2020; McGee et al., 2014; Schneider et al., 2014). During Heinrich Stadial 1 (HS1; ~14.7–19 ka BP; BP: before present) and Younger Dryas (YD, ~12.9–11.7 ka BP), precipitation decreases in Central America (Escobar et al., 2012), west African Sahel (McGee et al., 2013; Otto-Bliesner et al., 2014), Arabian Sea (Deplazes et al., 2013) and East and South Asia (Y. J. Wang et al., 2001; Yancheva et al., 2007) but increases in subtropical Brazil (Cruz et al., 2005; X. Wang et al., 2007), northern Australia (Ayliffe et al., 2013; Denniston et al., 2013), and the southern African tropics and subtropics (Konecky et al., 2011; Stager et al., 2011; also c.f. Figures 1a–1c). Such dipole-like rainfall changes indicate a southward shift of the intertropical convergence zone (ITCZ) (Arbuszewski et al., 2013; Gibbons et al., 2014), which coincides with a slowdown or shutdown of the Atlantic meridional overturning circulation (AMOC) triggered by the freshwater discharge due to ice sheet melts into the North Atlantic (Clark et al., 2001; McManus et al., 2004). It has been suggested that the weakened or nearly collapsed AMOC could cause a diminished northward oceanic heat transport across the Atlantic, which leads to a general cooling over the North Hemisphere and hence a southward displacement of the ITCZ during these periods (e.g., Arbuszewski et al., 2013; Gibbons et al., 2014; McGee et al., 2014).

Apart from the meltwater induced AMOC change, many other factors have also been put forward to explain the deglacial ITCZ migration. For example, slab ocean model results indicate that, without a change in ocean circulation, the deglacial decline in high-latitude ice sheets and sea ice could modify inter-hemispheric radiation balances at the top-of-atmosphere (TOA) (Chiang et al., 2003) and hence bring out a northward ITCZ shift from

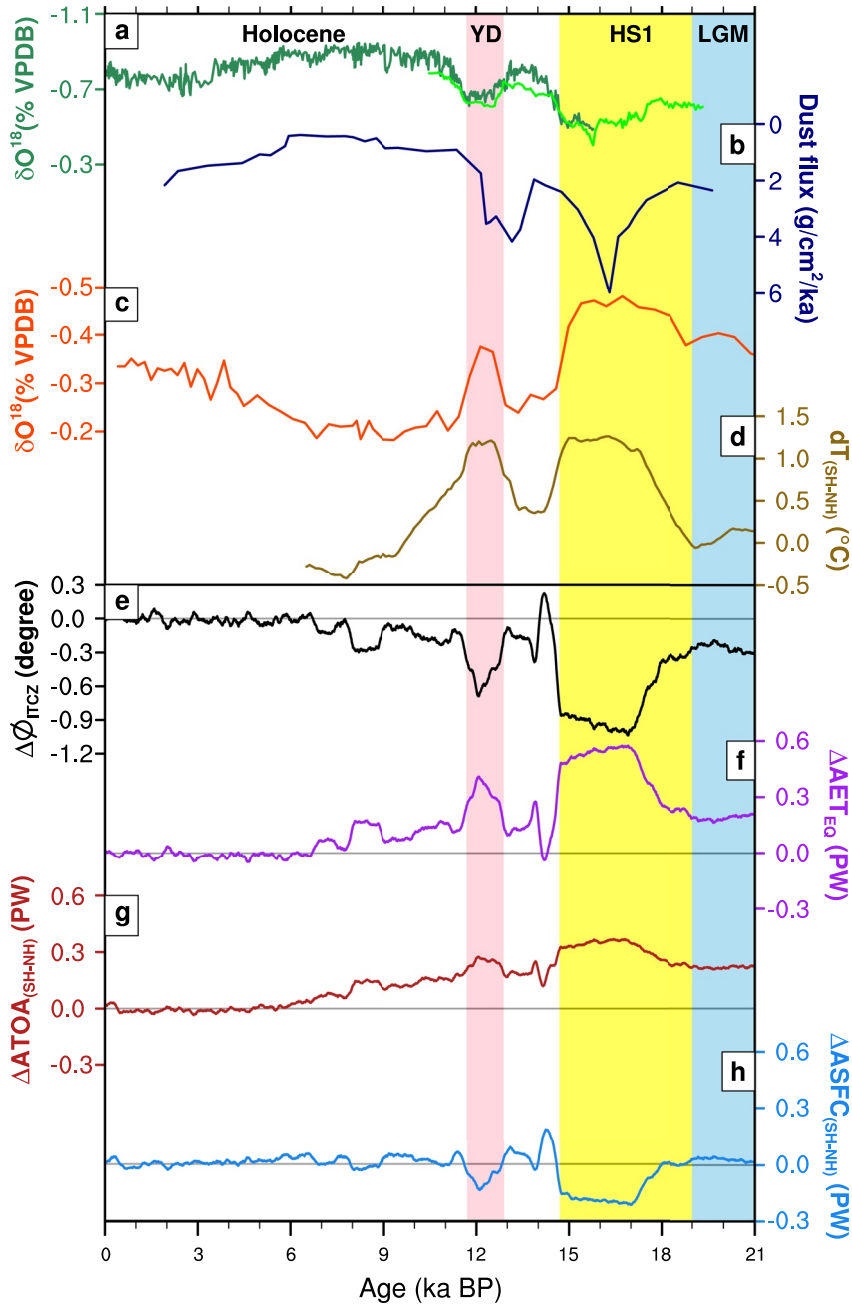

Figure 1. (a) Speleothem $\delta^{18}O$ from Dongge Cave (green) and Hulu Cave (light green) in China indicative of East Asia monsoon strength (Y. J. Wang et al., 2001; Yancheva et al., 2007). (b) Saharan dust deposition along the northwestern African margin (dark blue) indicative of summer precipitation and winter trade wind strengths (McGee et al., 2013). (c) Speleothem $\delta^{18}O$ from Botuvera Cave in southeast Brazil (orange) indicative of precipitation strength (X. Wang et al., 2007). (d) Reconstruction of area-weighted interhemispheric surface temperature contrast, that is, Southern Hemisphere minus Northern Hemisphere (Shakun et al., 2012). Changes in (e) global intertropical convergence zone latitudinal position (ϕ_{ITCZ}), (f) atmospheric cross-equatorial energy transport (AET_{EQ}) and interhemispheric asymmetries of (g) top-of-atmosphere radiation ($ATOA_{SH-NH}$) and (h) surface ($ASFC_{SH-NH}$) energy fluxes relative to near modern climate (1.1–3 ka BP) in TraCE-21 ka.

Last Glacial Maximum (LGM) to modern climate (Chiang & Bitz, 2005). Besides ice sheet retreats, orbit variations and rising atmospheric concentrations of long-lived greenhouse gases (GHGs) during the last deglaciation may also potentially modulate the position of the ITCZ (Clark et al., 2012; Cruz et al., 2005; Otto-Bliesner et al., 2014). These examples raise a scientific question that the deglacial change in global ITCZ could have been

driven by a myriad of climate feedbacks and physical processes far beyond the ocean circulation and heat transport changes in the Atlantic.

The atmospheric energetics framework (e.g., Kang, 2020; Kang et al., 2008; Schneider et al., 2014) helps address above scientific question. In this framework, changes in the ascending branch of the Hadley cell or the global ITCZ position (Figure 1e) are anti-correlated with changes in the atmospheric cross-equatorial energy transport (AET_{EQ}) (Figure 1f). Particularly, AET_{EQ} could be modified via either the inter-hemispheric asymmetry of TOA radiation energy fluxes ($ATOA_{SH-NH}$) (Figure 1g) or the inter-hemispheric asymmetry of surface energy fluxes ($ASFC_{SH-NH}$) (Figure 1h) that is approximately equal to global cross-equatorial oceanic heat transport ($GOHT_{EQ}$) over decadal or longer timescales (D. M. Frierson et al., 2013). Here we apply the atmospheric energetics framework to a simulation of Transient Climate Evolution over the last 21,000 years (TraCE-21ka) (Z. Liu et al., 2009) and accompanying single forcing experiments (F. He et al., 2013) with a fully coupled model to explore the mechanism driving the migration of global ITCZ during the last deglaciation.

2. Data and Methods

2.1. TraCE-21ka and Accompanying Single Forcing Experiments

TraCE-21ka and accompanying single forcing experiments are analyzed in this study to explore the transient ITCZ migration during the last 21,000 years. They are performed with a low-resolution version of Community Climate System Model Version 3 (CCSM3) that is a fully coupled model without flux adjustment (Yeager et al., 2006) but with a dynamic global vegetation module (Z. Liu et al., 2009). The atmosphere component of CCSM3 has a horizontal resolution of about 3.75° and 26 vertical hybrid coordinate levels and its ocean component has a nominal 3°horizontal resolution and 25 vertical levels. TraCE-21ka is forced by changes in orbital parameters, GHGs concentrations, meltwater fluxes and ice sheet extents, which can well simulate the climate changes during the last deglaciation (e.g., W. Liu & Hu, 2015; W. Liu et al., 2021, 2015). The ice sheet extents are obtained from ICE-5G (VM2) data (Peltier, 2004). TraCE-21ka is accompanied by four single-forcing simulations: TraCE-ORB, TraCE-GHG, TraCE-MWF and TraCE-ICE. In particular, TraCE-ORB and TraCE-GHG simulations are only forced by transient variation in orbital parameters and GHGs concentrations of the past 22,000 years, respectively, with all other forcings fixed at 22 ka BP levels. TraCE-MWF and TraCE-ICE simulations are only forced by transient variations in meltwater fluxes and ice sheets of the past 19,000 years, respectively, with all other forcings fixed at 19 ka BP levels. The transient variation of the prescribed forcing in a single-forcing experiment is identical to that applied to TraCE-21ka. Seen from the changes in the ITCZ and atmospheric cross-equatorial energy transport, the sum of single forcing experiments can well reproduce TraCE-21ka (Figure S1 in Supporting Information S1).

We employ the decadal annual mean outputs of TraCE-21ka and accompanying single forcing experiments, in which we calculate the changes relative to the 1.1–3 ka BP climatology, seeing that the output of sea ice model during 0–1.1 ka BP is not available in TraCE-MWF. In addition, we use decadal seasonal mean atmosphere outputs of TraCE-21ka to calculate the contributions of climate feedbacks to TOA radiation changes via the radiative kernel method (Shell et al., 2008; Soden et al., 2008). Relative to the 1.1–3 ka BP seasonal climatology, we first compute the change in the seasonal climatology during HS1 for the targetted variable and then times this change by the corresponding radiative kernel to assess the alteration in TOA radiation. Since the shortwave cloud feedback parameter depends on forcing and the water vapor and lapse rate feedback parameters depend on background climate state (Yoshimori et al., 2011), we only assess the contribution of the ice-albedo feedback in our study.

Additionally, we examine the iTraCE simulations during 11–20 ka BP with 1-degree iCESM1.3 (C. He et al., 2021), which follows a different experimental design from TraCE-21ka. Based on an experiment with altering ice sheets and ocean bathymetry (ICE), insolation (ICE + ORB), GHGs (ICE + ORB + GHG) and meltwater fluxes (ICE + ORB + GHG + MWF) successively added to the previous experiment, which form a series of iTraCE simulations. Accordingly, the response to each forcing can be extracted from ICE or the difference between one simulation and its prior simulation in the series. It is worth noting that the forings are different between TraCE-ICE and ICE in iTraCE, as the former includes only changes in ice sheets while the latter includes changes in both ice sheets and ocean bathymetry.

2.2. The Atmospheric Energetics Framework

The atmospheric energetics framework links atmospheric cross-equatorial energy transport (AET_{EQ}) to the Hadley cell and ITCZ (e.g., Kang, 2020; Kang et al., 2008; Schneider et al., 2014). The rationale is that moist static energy and water vapor centralize on the upper and lower troposphere in deep tropics such that they are transported by the Hadley cell in opposite directions. In another word, the displacements of the Hadley cell and hence the ITCZ are anti-correlated with the change in AET_{EQ}. On decadal or longer timescales when the temporal change of atmospheric energy is neglectable, AET_{EQ} can be calculated as

$$AET_{EQ} = ATOA_{SH-NH} - ASFC_{SH-NH} \tag{1}$$

where $ATOA_{SH-NH}$ and $ASFC_{SH-NH}$ are the differences of the hemispherical integrations of energy fluxes entering the TOA and the ocean/land surface between the Southern Hemisphere (SH) and Northern Hemisphere (NH), respectively. They are calculated as

$$ATOA_{SH-NH} = \frac{1}{2}\left[\int_{-\pi/2}^{0}\int_{0}^{2\pi} F_{TOA}a^2\cos(\phi')d\lambda d\phi' - \int_{0}^{\pi/2}\int_{0}^{2\pi} F_{TOA}a^2\cos(\phi')d\lambda d\phi'\right] \tag{2}$$

and

$$ASFC_{SH-NH} = \frac{1}{2}\left[\int_{-\pi/2}^{0}\int_{0}^{2\pi} F_{SFC}a^2\cos(\phi')d\lambda d\phi' - \int_{0}^{\pi/2}\int_{0}^{2\pi} F_{SFC}a^2\cos(\phi')d\lambda d\phi'\right] \tag{3}$$

where ϕ', λ and a denote latitude, longitude and the Erath's radius. F_{TOA} and F_{SFC} are energy fluxes at the TOA and at the ocean/land surface. Moreover, on decadal or longer timescales, the global cross-equatorial ocean heat transport ($GOHT_{EQ}$) is apporximately equal to $ASFC_{SH-NH}$, that is, $GOHT_{EQ} \approx ASFC_{SH-NH}$, seeing that the interhemispheric difference of ocean heat storage is neglectable (D. M. Frierson et al., 2013) when compared to either $GOHT_{EQ}$ or $ASFC_{SH-NH}$. As a result, the global cross-equatorial atmospheric energy transport and oceanic heat transport satisfy

$$AET_{EQ} \approx ATOA_{SH-NH} - GOHT_{EQ} \tag{4}$$

Besides, the location of global ITCZ (ϕ_{ITCZ}) can be estimated as the latitudinal centroid of precipitation:

$$\phi_{ITCZ} = \frac{\int_{\phi_1}^{\phi_2}\phi'\cos(\phi')P_r d\phi'}{\int_{\phi_1}^{\phi_2}\cos(\phi')P_r d\phi'} \tag{5}$$

where $\phi_1 = 20°S$ and $\phi_2 = 20°N$ are the latitudinal bounds for integration and P_r denotes annual mean precipitation (D. M. W. Frierson & Hwang, 2012).

3. Results

3.1. The Deglacial ITCZ Migration in Proxy Data and TraCE-21ka

We first compare the evolution patterns of global ITCZ during the last 21,000 years between proxy data and TraCE-21ka. We calculate the ITCZ change ($\Delta\phi_{ITCZ}$ where Δ indicates the change relative to 1.1–3 ka BP) from the near-modern climate in TraCE-21ka (Figure 1e). We find that TraCE-21ka well captures the main characteristics of deglacial ITCZ change as reflected by proxy records. Both model and proxy data show robust southward ITCZ displacements during HS1 and YD events (Figures 1a–1c and 1e) with rainfall decrease and increase to the north and south of equator (Figure S2 in Supporting Information S1), which correspond to strong northward ΔAET_{EQ} (Figures 1f and S3 in Supporting Information S1). They also illustrate a long-term trend of northward ITCZ migration from LGM to modern climate (Atwood et al., 2020; Donohoe et al., 2013), along with a declining trend of ΔAET_{EQ} during the last deglaciation (Figure 1f). Herein it merits attention that, besides ITCZ changes, other mechanisms such as variations in the intensity of the Indian monsoon (Pausata et al., 2011) have also been suggested to explain the Hulu Cave $\delta^{18}O$ change. Thereby, we further examine the evolution of interhemispheric temperature contrast based on surface temperature reconstructions (Shakun et al., 2012), which reveals a warmer

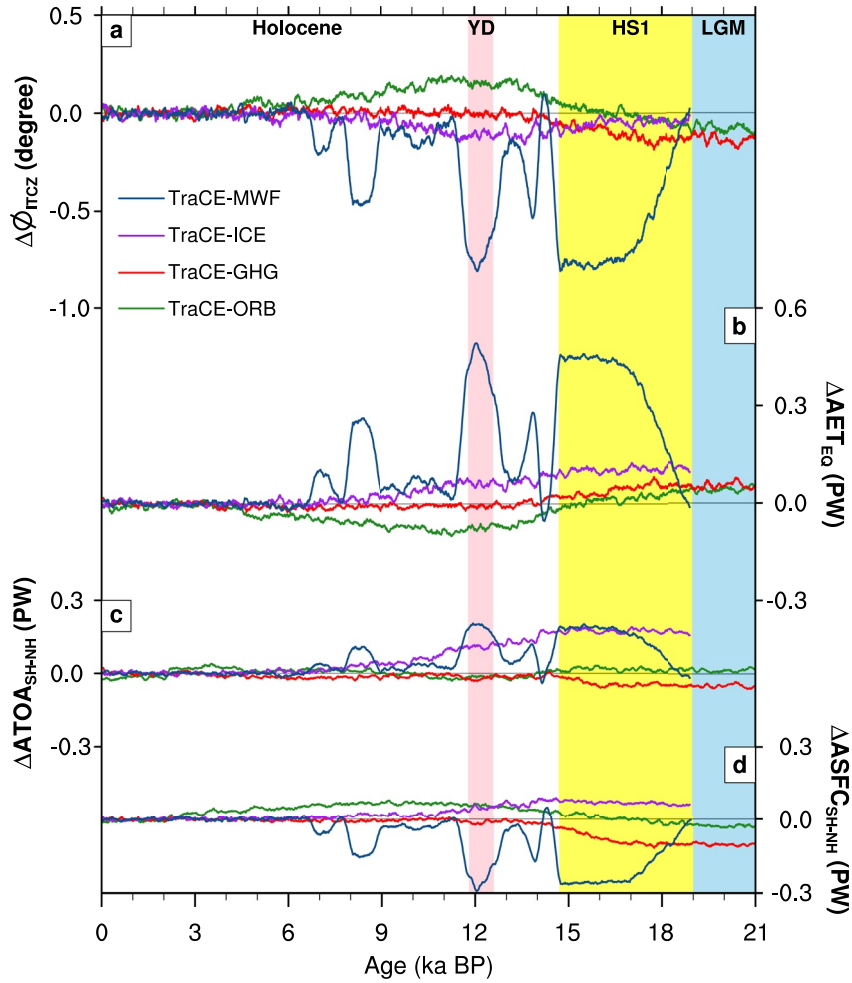

Figure 2. Changes in (a) global intertropical convergence zone latitudinal position (ϕ_{ITCZ}), (b) atmospheric cross-equatorial energy transport (AET_{EQ}) and interhemispheric asymmetries of (c) top-of-atmosphere radiation energy fluxes ($ATOA_{SH-NH}$) and (d) surface ($ASFC_{SH-NH}$) energy fluxes relative to near modern climate (1.1–3 ka BP) in the single forcing experiments of TraCE-MWF (blue), TraCE-ICE (purple), TraCE-GHG (red) and TraCE-ORB (green).

SH during HS1 and YD as well as a long-term trend of cooler SH than the NH between 21 and 6.5 ka BP (Figure 1d). Such interhemispheric temperature contrasts support aforementioned ITCZ changes since the ITCZ always tends to reside over the warmer hemisphere.

We further isolate and quantify the effects of various climate forcers—orbital, GHGs, ice sheet variations and meltwater into oceans—on deglacial ITCZ changes using the single-forcing experiments: TraCE-ORB, TraCE-GHG, TraCE-ICE and TraCE-MWF. We find that the meltwater forcing drives $\Delta\phi_{ITCZ}$ on average of −0.58° and −0.65° during HS1 and YD (Figure 2a), which correspond to ΔAET_{EQ} on average of 0.33 PW (1 PW = 10^{15} W) in HS1 and 0.39 PW in YD (Figure 2b). $\Delta ATOA_{SH-NH}$ contributes to ΔAET_{EQ} by 0.14 PW in HS1 and 0.17 PW in YD (Figure 2c) while $\Delta GOHT_{EQ}$ accounts for the rest of ΔAET_{EQ} (Figure 2d). This result suggests that changes in both inter-hemispheric TOA radiation asymmetry and global cross-equatorial oceanic heat transport are about equally important to the abrupt southward ITCZ shifts during HS1 and YD.

The meltwater forcing explains most of the abrupt southward displacements of global ITCZ during HS1 and YD while orbital variations, rising atmospheric GHG concentrations and receding ice sheets are primarily responsible for the long-term ITCZ trend (Figure 2a). Specifically, orbital variations drive a gradual northward ITCZ migration and a declining trend of ΔAET_{EQ} from the LGM to early Holocene (around 10 ka BP) but a southward ITCZ migration and an increasing trend of ΔAET_{EQ} afterward (Figures 2a and 2b). Through the last deglaciation, orbital variations overall contribute to a net northward ITCZ displacement. GHG increases and ice sheet

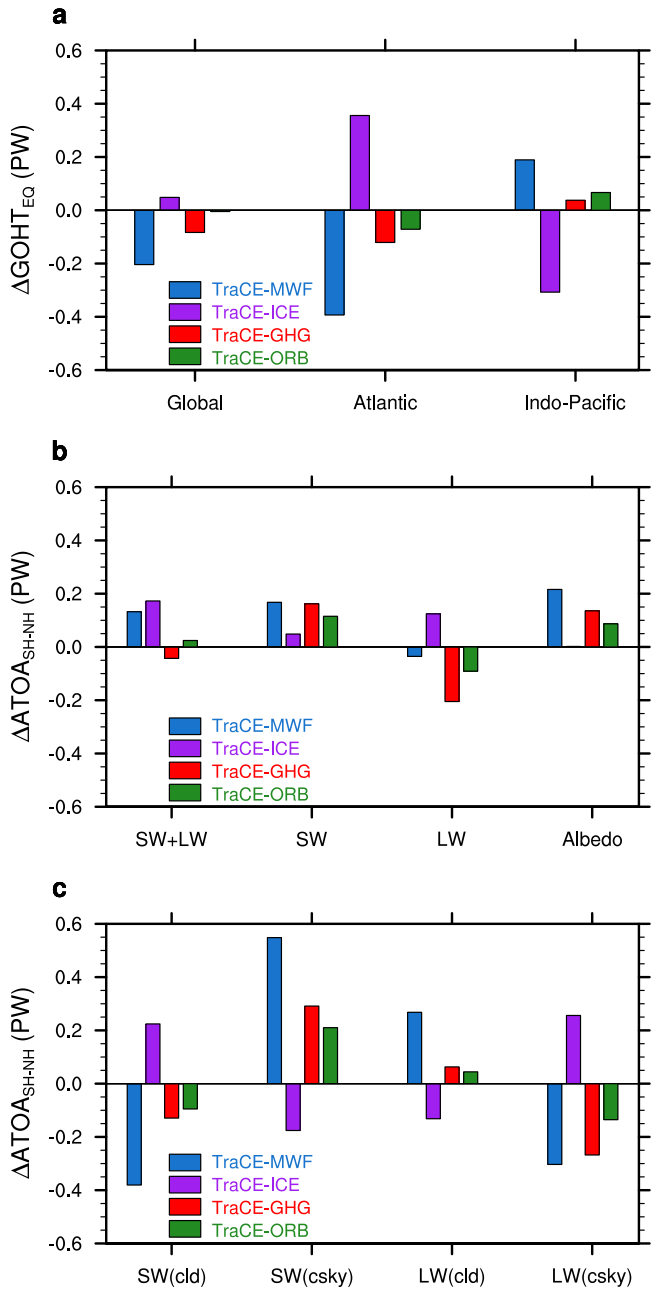

Figure 3. (a) Change in global, Atlantic and Indo-Pacific oceanic cross-equatorial heat transports during Heinrich Stadial 1 (HS1) relative to 1.1–3 ka BP in TraCE single forcing experiments. (b) Changes in the interhemispheric asymmetries of net (shortwave plus longwave), shortwave and longwave radiation at the top-of-atmosphere (TOA) and the contribution to TOA radiation asymmetry from the ice-albedo feedback during HS1 relative to 1.1–3 ka BP in TraCE single forcing experiments. (c) Same as panel (b) but for cloud-affected (cld) and clear-sky (csky) shortwave and longwave radiation. SW = SW(cld) + SW(csky) and LW = LW(cld) + LW(csky).

retreats generally contribute to the long-term trend of northward ITCZ shift and ΔAET_{EQ} decline through the last deglaciation (Figures 2a and 2b). The effect from GHG increases is most robust prior to YD while the effect from ice sheet retreats lasts till Holocene.

We investigate the causes for the changes in global oceanic heat transport and TOA radiation asymmetry in the single-forcing experiments. Our analysis primarily focuses on HS1 because it is the period showing not only an abrupt southward ITCZ displacement in TraCE-MWF and but also southward ITCZ displacements relative to modern climate in TraCE-ICE, TraCE-ORB and TraCE-GHG. Finding the reason for the latter ITCZ displacements will help understand the long-term ITCZ trends—the overall northward deglacial ITCZ shifts— in these experiments. Our analysis shows that, in TraCE-MWF, the Laurentide ice sheet induced meltwater into the Northern Atlantic suppresses the formation of North Atlantic deep water and heavily weakens the AMOC (Figure S4 in Supporting Information S1) and associated oceanic heat transport (Figure S5 in Supporting Information S1), which leads to a negative Atlantic ΔOHT_{EQ} of about −0.39 PW (Figure 3a). Meanwhile, due to inter-basin exchange (Jones & Cessi, 2016; Sun et al., 2020; Talley, 2013), an anomalous anticlockwise MOC is generated in the Indo-Pacific basin (Figure S4 in Supporting Information S1), along with alterations in Antarctic bottom water and diapycnal upwelling there (C. Zhu et al., 2021). This MOC change engenders a positive Indo-Pacific ΔOHT_{EQ} of 0.19 PW, which compensates about half of Atlantic ΔOHT_{EQ} and results in a negative $\Delta GOHT_{EQ}$ of −0.20 PW.

We also probe the interhemispheric TOA radiation asymmetry in TraCE-MWF during HS1 and find that the asymmetry is mostly driven by the changes in TOA shortwave radiation (Figure 3b). The clear-sky shortwave radiation shows general negative and positive anomalies in the Northern and Southern Hemispheres in response to meltwater forcing (Figure 4a). The largest radiation changes occur in the sea ice region over the subpolar North Atlantic and Southern Ocean where cloud effects partially offset the changes in the clear-sky shortwave radiation (Figure 4c). Integrated over the hemispheres, the total (clear-sky plus cloud-induced) shortwave radiation changes create an interhemispheric asymmetry of 0.17 PW (Figures 3b and 3c). On the other hand, the clear-sky longwave radiation exhibits general positive (downward) anomalies over the subpolar North Atlantic (Figure S6c in Supporting Information S1), which is related to the surface cooling in the subpolar North Atlantic (Figure S7a in Supporting Information S1) that engenders reduced outgoing (upward) clear-sky longwave radiation fluxes. Cloud effects, on the other hand, induce negative anomalies of longwave radiation over the subpolar North Atlantic and around the Central America (Figure S6e in Supporting Information S1), which largely compensate the change in clear-sky longwave radiation. Integrated over the hemispheres, the total longwave radiation changes create an interhemispheric asymmetry of 0.03 PW (Figures 3b and 3c). As a result, the changes in shortwave radiation are slightly compensated by the changes in longwave radiation, which leads to a $\Delta ATOA_{SH-NH}$ of 0.13 PW (Figure 3b).

We further employ the radiative kernel method to quantify the contribution of the surface albedo feedback to interhemispheric TOA radiation asymmetry. We find that, via the surface albedo feedback, the expanded Arctic sea ice in the Atlantic sector (Figure S8 in Supporting Information S1) generates an anomalous TOA radiative cooling over the subpolar Atlantic while the declined Antarctic sea ice (Figure S8 in Supporting Information S1) produces an anomalous TOA radiative

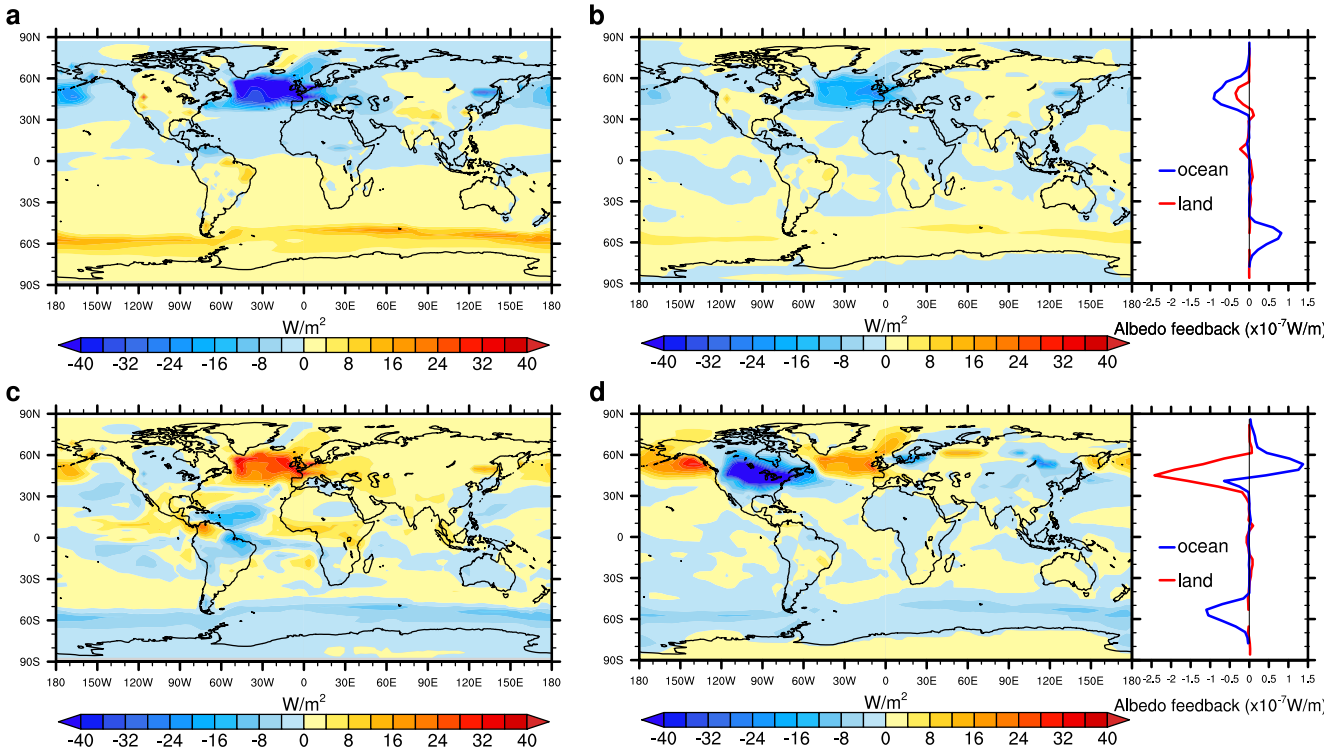

Figure 4. (left column) Maps of the changes in top-of-atmosphere (TOA) (a) clear-sky and (c) cloud-affected shortwave radiation during Heinrich Stadial 1 (HS1) relative to 1.1–3 ka BP in TraCE-MWF. The cloud-affected shortwave radiation is calculated as the difference between the toal and clear-sky shortwave radiation. (right column) Maps of the contribution of the ice-albedo feedback to TOA radiation changes and contributions of the ice-albedo feedback on TOA radiation changes on individual latitudes integrated over land (red) and over ocean (blue) during HS1 relative to 1.1–3 ka BP in (b) TraCE-MWF and (d) TraCE-ICE. Downward positive for all the panels.

warming over the Southern Ocean (Figure 4b), both of which contribute to an interhemispheric TOA radiation asymmetry as large as 0.22 PW (Figure 3b).

Besides TraCE-MWF, TraCE-ICE also simulates a $\Delta ATOA_{SH-NH}$ of 0.17 PW during HS1. However, unlike the meltwater scenario, this TOA radiation asymmetry is contributed primarily by the asymmetry of longwave radiation and secondly by the asymmetry of shortwave radiation (Figure 3b). The clear-sky longwave radiation shows strong positive (downward) anomalies over the North America and Antarctic but negative (downward) anomalies over the North Pacific and Atlantic Oceans (Figure S6d in Supporting Information S1), which is related to surface cooling in the former locations but surface warming in the latter (Figure S7b in Supporting Information S1) that diminishes and promotes outgoing (upward) clear-sky longwave radiation fluxes. The surface cooling and warming, moreover, are closely tied to the changes in land ice and sea ice in these regions (Figure S8 in Supporting Information S1). Meanwhile, cloud effects induce a partial compensation of above clear-sky longwave radiation anomalies (Figure S6f in Supporting Information S1). Integrated over the hemispheres, the total longwave radiation change contributes to $\Delta ATOA_{SH-NH}$ by 0.12 PW (Figure 3b).

It is worth noting that the surface albedo feedback plays a minimal role in promoting the interhemispheric TOA radiation asymmetry in TraCE-ICE (Figure 3b). Albeit the existing Laurentide ice sheet during HS1 causes an anomalous positive land surface albedo relative to modern climate, the dwindled Arctic sea ice in both Atlantic and Pacific sectors (along with a stronger AMOC, a point to return later; Figure S8 in Supporting Information S1) gives rise to an anomalous negative surface albedo in ocean. The compensation between these land and ocean albedo changes results in an anomalous TOA radiation of −0.19 PW in the NH. Meanwhile, the expansion of Antarctic sea ice brings out an anomalous positive surface albedo in ocean, leading to an anomalous TOA radiation of −0.19 PW in the SH (Figure 4d). As a result, the surface albedo feedback has an around zero contribution to $\Delta ATOA_{SH-NH}$ (Figure 3b).

Though TraCE-ICE shows a $\Delta ATOA_{SH-NH}$ that is comparable to or even slightly larger than that in TraCE-MWF during HS1 (Figure 3b), its ITCZ shift has a much smaller amplitude than the latter (Figure 2a). This is because the deglacial retreat of ice sheets has been suggested to weaken the AMOC by modulating the northern westerly winds and associated sea-ice transports (J. Zhu et al., 2014) such that the AMOC is stronger during HS1 than modern climate in TraCE-ICE (Figure S4 in Supporting Information S1). This stronger AMOC induces a northward ΔOHT_{EQ} of 0.36 PW in the Atlantic basin, which is mostly compensated by the southward ΔOHT_{EQ} in the Indo-Pacific (Figure 3a) primarily induced by an anomalous anticlockwise MOC there (Figure S4 in Supporting Information S1). As a result, $\Delta GOHT_{EQ}$ shows an increase of 0.05 PW in HS1 (Figure 3a), which partially offsets $\Delta ATOA_{SH-NH}$ to reduce the magnitude of the northward ΔAET_{EQ} and southward ITCZ shift during this period.

In addition, TraCE-ORB shows a weak southward ITCZ displacement and a weaker northward ΔAET_{EQ} during HS1 under orbital forcing (Figure 2). The northward ΔAET_{EQ} mainly comes from $\Delta ATOA_{SH-NH}$ (Figure 3b), since $\Delta GOHT_{EQ}$ is close to zero as a result of a perfect cancellation between Atlantic and Indo-Pacific ΔOHT_{EQ} (Figure 3a). By contrast, in TraCE-GHG, the northward ΔAET_{EQ} during HS1 is mainly owing to a weaker-than-today AMOC (J. Zhu et al., 2015, also c.f. Figure S4 in Supporting Information S1) and associated oceanic heat transport under GHG forcing (Figure S5 in Supporting Information S1). The strong negative Atlantic ΔOHT_{EQ} overwhelms the compensations from Indo-Pacific ΔOHT_{EQ} (Figure 3a) and $\Delta ATOA_{SH-NH}$ (Figure 3b) and hence accounts for the northward ΔAET_{EQ} and southward ITCZ displacement.

4. Conclusion and Discussion

TraCE-21ka and accompanying single forcing experiments suggest that the abrupt southward ITCZ shifts during HS1 and YD are mainly driven by ice-sheet-induced meltwater forcing while the long-term trend of northward ITCZ migration from LGM to modern climate can be attributed to orbital variations, rising atmospheric GHGs and ice sheet retreats during the last deglaciation. Our atmospheric energetics analysis shows that, under meltwater forcing, not only the declined AMOC and associated Atlantic heat transport but also inter-hemispheric TOA radiation asymmetry is important to the southward ITCZ shift during HS1. Moreover, changes in the overturning circulation and associated heat transport in the Indo-Pacific merit attentions, since the latter change can effectively compensate about half of the Atlantic heat transport change at the equator. Benefitted from the interactive sea ice physics and ocean dynamics in the TraCE experiments, we show a muted surface albedo feedback induced by deglacial ice sheet changes, which is different from previous slab ocean model and adds new insights to our understanding of the role of ice sheet change on deglacial ITCZ migration.

Besides, we calculate the latitude of global ITCZ (ϕ_{ITCZ}) and cross-equatorial atmospheric energy transport (AET_{EQ}) during 11–20 ka BP in iTraCE simulations. Note here a direct comparison between TraCE-21ka and iTraCE cannot be made since iTraCE lacks modern or late Holocene state as a control for each single forcing. We find that the abrupt southward shifts of the ITCZ driven by meltwater during HS1 and YD are also evident in iTraCE, which correspond to northward AET_{EQ} (Figure S9 in Supporting Information S1). However, we cannot estimate the long-term trend of ITCZ migration throughout the last deglacial given iTraCE simulations cut off at 11 ka.

Data Availability Statement

Data of TraCE-21ka and accompanying single forcing experiments are available at https://www.earthsystemgrid.org/project/trace.html.

Acknowledgments
This work is supported by grants to W. Liu from U.S. National Science Foundation (AGS-2053121 and OCE-2123422). W. Liu is also supported by the Alfred P. Sloan Foundation as a Research Fellow and by the Hellman Fellows Fund as a Hellman Fellow. S. Li performed the analysis and wrote the original draft of the manuscript. W. Liu conceived the study and made substantial improvements to the manuscript. Both authors contributed to interpreting the results.

References

Arbuszewski, J. A., Demenocal, P. B., Cléroux, C., Bradtmiller, L., & Mix, A. (2013). Meridional shifts of the Atlantic intertropical convergence zone since the Last Glacial Maximum. *Nature Geoscience*, *6*(11), 959–962. https://doi.org/10.1038/ngeo1961

Atwood, A. R., Donohoe, A., Battisti, D. S., Liu, X., & Pausata, F. S. (2020). Robust longitudinally variable responses of the ITCZ to a myriad of climate forcings. *Geophysical Research Letters*, *47*(17), e2020GL088833. https://doi.org/10.1029/2020gl088833

Ayliffe, L. K., Gagan, M. K., Zhao, J. X., Drysdale, R. N., Hellstrom, J. C., Hantoro, W. S., et al. (2013). Rapid interhemispheric climate links via the Australasian monsoon during the last deglaciation. *Nature Communications*, *4*, 1–6. https://doi.org/10.1038/ncomms3908

Chiang, J. C., Biasutti, M., & Battisti, D. S. (2003). Sensitivity of the Atlantic intertropical convergence zone to Last Glacial Maximum boundary conditions. *Paleoceanography*, *18*(4), 1094. https://doi.org/10.1029/2003pa000916

Chiang, J. C., & Bitz, C. M. (2005). Influence of high latitude ice cover on the marine Intertropical Convergence Zone. *Climate Dynamics*, *25*(5), 477–496. https://doi.org/10.1007/s00382-005-0040-5

Clark, P. U., Marshall, S. J., Clarke, G. K., Hostetler, S. W., Licciardi, J. M., & Teller, J. T. (2001). Freshwater forcing of abrupt climate change during the last glaciation. *Science*, *293*(5528), 283–287. https://doi.org/10.1126/science.1062517

Clark, P. U., Shakun, J. D., Baker, P. A., Bartlein, P. J., Brewer, S., Brook, E., et al. (2012). Global climate evolution during the last deglaciation. *Proceedings of the National Academy of Sciences of the United States of America*, *109*(19), E1134–E1142. https://doi.org/10.1073/pnas.1116619109

Cruz, F. W., Burns, S. J., Karmann, I., Sharp, W. D., Vuille, M., Cardoso, A. O., et al. (2005). Insolation-driven changes in atmospheric circulation over the past 116,000 years in subtropical Brazil. *Nature*, *434*(7029), 63–66. https://doi.org/10.1038/nature03365

Denniston, R. F., Wyrwoll, K. H., Asmerom, Y., Polyak, V. J., Humphreys, W. F., Cugley, J., et al. (2013). North Atlantic forcing of millennial-scale Indo-Australian monsoon dynamics during the Last Glacial Period. *Quaternary Science Reviews*, *72*, 159–168. https://doi.org/10.1016/j.quascirev.2013.04.012

Deplazes, G., Lückge, A., Peterson, L. C., Timmermann, A., Hamann, Y., Hughen, K. A., et al. (2013). Links between tropical rainfall and North Atlantic climate during the Last Glacial Period. *Nature Geoscience*, *6*(3), 213–217. https://doi.org/10.1038/ngeo1712

Donohoe, A., Marshall, J., Ferreira, D., & McGee, D. (2013). The relationship between ITCZ location and atmospheric heat transport across the equator: From the seasonal cycle to the Last Glacial Maximum. *Journal of Climate*, *26*(11), 3597–3618. https://doi.org/10.1175/jcli-d-12-00467.1

Escobar, J., Hodell, D. A., Brenner, M., Curtis, J. H., Gilli, A., Mueller, A. D., et al. (2012). A ~43-ka record of paleoenvironmental change in the Central American lowlands inferred from stable isotopes of lacustrine ostracods. *Quaternary Science Reviews*, *37*, 92–104. https://doi.org/10.1016/j.quascirev.2012.01.020

Frierson, D. M., Hwang, Y. T., Fučkar, N. S., Seager, R., Kang, S. M., Donohoe, A., et al. (2013). Contribution of ocean overturning circulation to tropical rainfall peak in the Northern Hemisphere. *Nature Geoscience*, *6*(11), 940–944. https://doi.org/10.1038/ngeo1987

Frierson, D. M. W., & Hwang, Y.-T. (2012). Extratropical influence on ITCZ shifts in slab ocean simulations of global warming. *Journal of Climate*, *25*(2), 720–733. https://doi.org/10.1175/jcli-d-11-00116.1

Geen, R., Bordoni, S., Battisti, D. S., & Hui, K. (2020). Monsoons, ITCZs, and the concept of the global monsoon. *Reviews of Geophysics*, *58*(4), e2020RG000700. https://doi.org/10.1029/2020rg000700

Gibbons, F. T., Oppo, D. W., Mohtadi, M., Rosenthal, Y., Cheng, J., Liu, Z., & Linsley, B. K. (2014). Deglacial $\delta^{18}O$ and hydrologic variability in the tropical Pacific and Indian Oceans. *Earth and Planetary Science Letters*, *387*, 240–251. https://doi.org/10.1016/j.epsl.2013.11.032

He, C., Liu, Z., Otto-Bliesner, B. L., Brady, E. C., Zhu, C., Tomas, R., et al. (2021). Hydroclimate footprint of pan-Asian monsoon water isotope during the last deglaciation. *Science Advances*, *7*(4), eabe2611. https://doi.org/10.1126/sciadv.abe2611

He, F., Shakun, J. D., Clark, P. U., Carlson, A. E., Liu, Z., Otto-Bliesner, B. L., & Kutzbach, J. E. (2013). Northern Hemisphere forcing of Southern Hemisphere climate during the last deglaciation. *Nature*, *494*(7435), 81–85. https://doi.org/10.1038/nature11822

Jones, C. S., & Cessi, P. (2016). Interbasin transport of the meridional overturning circulation. *Journal of Physical Oceanography*, *46*(4), 1157–1169. https://doi.org/10.1175/jpo-d-15-0197.1

Kang, S. M. (2020). Extratropical influence on the tropical rainfall distribution. *Current Climate Change Reports*, *6*(1), 24–36. https://doi.org/10.1007/s40641-020-00154-y

Kang, S. M., Held, I. M., Frierson, D. M. W., & Zhao, M. (2008). The response of the ITCZ to extratropical thermal forcing: Idealized slab-ocean experiments with a GCM. *Journal of Climate*, *21*(14), 3521–3532. https://doi.org/10.1175/2007jcli2146.1

Konecky, B. L., Russell, J. M., Johnson, T. C., Brown, E. T., Berke, M. A., Werne, J. P., & Huang, Y. (2011). Atmospheric circulation patterns during late Pleistocene climate changes at Lake Malawi, Africa. *Earth and Planetary Science Letters*, *312*(3–4), 318–326. https://doi.org/10.1016/j.epsl.2011.10.020

Liu, W., & Hu, A. (2015). The role of the PMOC in modulating the deglacial shift of the ITCZ. *Climate Dynamics*, *45*(11–12), 3019–3034. https://doi.org/10.1007/s00382-015-2520-6

Liu, W., Liu, Z., Cheng, J., & Hu, H. (2015). On the stability of the Atlantic meridional overturning circulation during the last deglaciation. *Climate Dynamics*, *44*(5–6), 1257–1275. https://doi.org/10.1007/s00382-014-2153-1

Liu, W., Liu, Z., & Li, S. (2021). The driving mechanisms on Southern Ocean upwelling change during the last deglaciation. *Geosciences*, *11*(7), 266. https://doi.org/10.3390/geosciences11070266

Liu, Z., Otto-Bliesner, B. L., He, F., Brady, E. C., Tomas, R., Clark, P. U., et al. (2009). Transient simulation of last deglaciation with a new mechanism for Bølling-Allerød warming. *Science*, *325*(5938), 310–314. https://doi.org/10.1126/science.1171041

McGee, D., deMenocal, P. B., Winckler, G., Stuut, J. B. W., & Bradtmiller, L. I. (2013). The magnitude, timing and abruptness of changes in North African dust deposition over the last 20,000 yr. *Earth and Planetary Science Letters*, *371*, 163–176. https://doi.org/10.1016/j.epsl.2013.03.054

McGee, D., Donohoe, A., Marshall, J., & Ferreira, D. (2014). Changes in ITCZ location and cross-equatorial heat transport at the Last Glacial Maximum, Heinrich Stadial 1, and the mid-Holocene. *Earth and Planetary Science Letters*, *390*, 69–79. https://doi.org/10.1016/j.epsl.2013.12.043

McManus, J. F., Francois, R., Gherardi, J. M., Keigwin, L. D., & Brown-Leger, S. (2004). Collapse and rapid resumption of Atlantic meridional circulation linked to deglacial climate changes. *Nature*, *428*(6985), 834–837. https://doi.org/10.1038/nature02494

Otto-Bliesner, B. L., Russell, J. M., Clark, P. U., Liu, Z., Overpeck, J. T., Konecky, B., et al. (2014). Coherent changes of southeastern equatorial and northern African rainfall during the last deglaciation. *Science*, *346*(6214), 1223–1227. https://doi.org/10.1126/science.1259531

Pausata, F. S. R., Battisti, D. S., Nisancioglu, K. H., & Bitz, C. M. (2011). Chinese stalagmite $\delta^{18}O$ controlled by changes in the Indian monsoon during a simulated Heinrich event. *Nature Geoscience*, *4*(7), 474–480. https://doi.org/10.1038/ngeo1169

Peltier, W. R. (2004). Global glacial isostasy and the surface of the ice-age Earth: The ICE-5G (VM2) model and GRACE. *Annual Review of Earth and Planetary Sciences*, *32*(1), 111–149. https://doi.org/10.1146/annurev.earth.32.082503.144359

Schneider, T., Bischoff, T., & Haug, G. H. (2014). Migrations and dynamics of the intertropical convergence zone. *Nature*, *513*(7516), 45–53. https://doi.org/10.1038/nature13636

Shakun, J. D., Clark, P. U., He, F., Marcott, S. A., Mix, A. C., Liu, Z., et al. (2012). Global warming preceded by increasing carbon dioxide concentrations during the last deglaciation. *Nature*, *484*(7392), 49–54. https://doi.org/10.1038/nature10915

Shell, K. M., Kiehl, J. T., & Shields, C. A. (2008). Using the radiative kernel technique to calculate climate feedbacks in NCAR's Community Atmospheric Model. *Journal of Climate*, *21*(10), 2269–2282. https://doi.org/10.1175/2007jcli2044.1

Soden, B. J., Held, I. M., Colman, R., Shell, K. M., Kiehl, J. T., & Shields, C. A. (2008). Quantifying climate feedbacks using radiative kernels. *Journal of Climate*, *21*(14), 3504–3520. https://doi.org/10.1175/2007jcli2110.1

Stager, J. C., Ryves, D. B., Chase, B. M., & Pausata, F. S. (2011). Catastrophic drought in the Afro-Asian monsoon region during Heinrich event 1. *Science*, *331*(6022), 1299–1302. https://doi.org/10.1126/science.1198322

Sun, S., Thompson, A. F., & Eisenman, I. (2020). Transient overturning compensation between Atlantic and Indo-Pacific basins. *Journal of Physical Oceanography*, *50*(8), 2151–2172. https://doi.org/10.1175/jpo-d-20-0060.1

Talley, L. D. (2013). Closure of the global overturning circulation through the Indian, Pacific, and Southern Oceans: Schematics and transports. *Oceanography*, *26*(1), 80–97. https://doi.org/10.5670/oceanog.2013.07

Wang, X., Auler, A. S., Edwards, R. L., Cheng, H., Ito, E., Wang, Y., et al. (2007). Millennial-scale precipitation changes in southern Brazil over the past 90,000 years. *Geophysical Research Letters*, *34*(23), L23701. https://doi.org/10.1029/2007gl031149

Wang, Y. J., Cheng, H., Edwards, R. L., An, Z. S., Wu, J. Y., Shen, C. C., & Dorale, J. A. (2001). A high-resolution absolute-dated late Pleistocene monsoon record from Hulu Cave, China. *Science*, *294*(5550), 2345–2348. https://doi.org/10.1126/science.1064618

Yancheva, G., Nowaczyk, N. R., Mingram, J., Dulski, P., Schettler, G., Negendank, J. F., et al. (2007). Influence of the intertropical convergence zone on the East Asian monsoon. *Nature*, *445*(7123), 74–77. https://doi.org/10.1038/nature05431

Yeager, S. G., Shields, C. A., Large, W. G., & Hack, J. J. (2006). The low-resolution CCSM3. *Journal of Climate*, *19*(11), 2545–2566. https://doi.org/10.1175/jcli3744.1

Yoshimori, M., Hargreaves, J. C., Annan, J. D., Yokohata, T., & Abe-Ouchi, A. (2011). Dependency of feedbacks on forcing and climate state in physics parameter ensembles. *Journal of Climate*, *24*, 6440–6455. https://doi.org/10.1175/2011jcli3954.1

Zhu, C., Liu, Z., Zhang, S., & Wu, L. (2021). Global oceanic overturning circulation forced by the competition between greenhouse gases and continental ice sheets during the last deglaciation. *Journal of Climate*, *34*(18), 7555–7570. https://doi.org/10.1175/jcli-d-21-0125.1

Zhu, J., Liu, Z., Zhang, J., & Liu, W. (2015). AMOC response to global warming: Dependence on the background climate and response timescale. *Climate Dynamics*, *44*(11–12), 3449–3468. https://doi.org/10.1007/s00382-014-2165-x

Zhu, J., Liu, Z., Zhang, X., Eisenman, I., & Liu, W. (2014). Linear weakening of the AMOC in response to receding glacial ice sheets in CCSM3. *Geophysical Research Letters*, *41*(17), 6252–6258. https://doi.org/10.1002/2014gl060891